



# Noise Reduction Method for Partial Discharge Fluorescence Fiber Sensors Based on Optimized Empirical Wavelet Transform

Chengyong Hu , Yi Huang , *Member, IEEE*, Chuanlu Deng , Ming Jia, Qi Zhang , *Member, IEEE*, Peng Wu, Yuncai Lu, Qun Li, Xiaobei Zhang , *Member, IEEE*, and Tingyun Wang , *Member, IEEE*

**Abstract**—A novel self-adaptive denoising method utilizing optimized empirical wavelet transform (EWT) is proposed to enhance the sensitivity of partial discharge (PD) fluorescence fiber sensors. The optimized EWT enhances the spectrum segmentation capability of conventional EWT via spectral kurtosis (SK). The SK at the optimal window length of noisy PD fluorescence signal is calculated to determine compact support of the Fourier spectrum for subsequent signal decomposition. Frequency components with SK value over the statistic threshold are used to rebuild the PD fluorescence signal. Subsequently, residual noise in the reconstructed signal is removed through adaptive wavelet threshold denoising. To evaluate the performance of the proposed method in denoising numerically simulated and experimentally obtained noisy PD fluorescence signals, outcomes are compared to those of the novel adaptive ensemble empirical mode decomposition (NAEEMD) method, EWT method, EWT joint with kurtogram (KEWT) method, and correlation spectral negentropy (CSNE)-based method. Quantitative metrics and running time are used to assess denoising performance and execution efficiency, respectively. Simulated and experimental results demonstrate that the proposed method possesses a superior noise reduction effect compared to the other four methods while restoring the detail of the PD fluorescence signal flooded by serious noise and consuming reduced computational cost.

**Index Terms**—Fluorescence fiber sensors, partial discharge detection, signal denoising, empirical wavelet transform (EWT), spectral kurtosis (SK).

## I. INTRODUCTION

**P**ARTIAL discharge (PD) detection is one of the efficient ways to assess insulation conditions of high-voltage apparatus, which can ensure their normal operation [1], [2]. There have been several PD detection methods that are widely utilized

[3], [4], [5], [6], including the pulse current method, ultrahigh-frequency method, acoustic emission method, and optical detection method. It is challenging to detect PD signals by utilizing conventional electrical methods, since many types of noises from the field environment, such as electromagnetic interference (EMI) and radio, etc., may be coupled with detection results, resulting in inaccuracy of PD detection [7]. Fortunately, the optical detection method based on fluorescence fiber sensors is capable of isolating most of the noise, due to insulation and immunity to the EMI of optical fibers [8], [9], [10]. Although the signals of fluorescence fiber sensors are immune to direct electrical and acoustic interference, they are still impacted by white noise from the photoelectric conversion of photomultiplier tubes (PMT), resulting in limited sensitivity or accuracy of fluorescence fiber sensors. Therefore, noise suppression of PD fluorescence signals is conducive to further application of fluorescence fiber sensors in the realm of PD detection.

Despite tremendous research efforts in signal decomposition-based PD signal denoising methods of conventional electrical sensors, there has been minimal published research on the noise reduction of PD fluorescence fiber sensors. Fluorescence PD signals can be denoised in analogous ways to PD signals from electrical sensors because they are somewhat similar to each other. Wavelet transform (WT) is one of the most widely employed methods for PD signal denoising [11], [12], due to the properties of multi-scale time-frequency analysis [13]. However, a major obstacle that restricts the practical application of WT is the requirement to manually select basis functions and decomposition levels. To adaptively decompose signals, the empirical mode decomposition (EMD) method has been proposed for PD signal denoising [14], [15]. Without the need for predefined basis functions and decomposition levels, EMD decomposes noisy PD signals into a set of intrinsic mode functions in order. Nevertheless, it is worth noting that EMD is vulnerable to modal mixing issues, as well as lacking mathematical theory. Various EMD-based variants of the methods [16], [17], [18] have addressed the modal mixing issue, the majority of which employ the noise-assisted approach. Due to multiple additions of white noise, these variant EMD-based methods suffer from residual-assisted noise impact as well as a considerably higher computational cost problem. Empirical wavelet transform (EWT) is an adaptive data-driven signal decomposition approach that integrates properties of EMD and WT while overcoming their issues [19]. Some researchers [20], [21] applied EWT to remove

Manuscript received 27 June 2024; accepted 3 July 2024. Date of publication 8 July 2024; date of current version 16 July 2024. This work was supported by the National Key Research and Development Program of China under Grant 2022YFF0708400. (*Corresponding author: Tingyun Wang.*)

Chengyong Hu, Yi Huang, Chuanlu Deng, Ming Jia, Qi Zhang, Xiaobei Zhang, and Tingyun Wang are with the Key Laboratory of Specialty Fiber Optics and Optical Access Networks, Joint International Research Laboratory of Specialty Fiber Optics and Advanced Communication, Shanghai University, Shanghai 200444, China (e-mail: desert\_hey@163.com; huangyi1008@shu.edu.cn; chuanludeng@163.com; jiaming2687@shu.edu.cn; qzhang9@shu.edu.cn; xbzhang@shu.edu.cn; tywang@shu.edu.cn).

Peng Wu, Yuncai Lu, and Qun Li are with State Grid Jiangsu Electric Power Research Institute, Nanjing 211103, China (e-mail: varletwp@163.com; sixhair@163.com; qun\_li@sina.com).

Digital Object Identifier 10.1109/JPHOT.2024.3424439

white noise from noisy PD signals, and the results demonstrate that these EWT-based methods have excellent anti-modal mixing properties and denoising performance. Yet, since the spectrum division approach of EWT is dependent on local minima, noise will alter their distribution [22], resulting in the decomposition of redundant mode components and significant calculation cost.

Spectral kurtosis (SK) is a statistics tool that can identify the presence of a transitory signal as well as the band in which the signal appears [23], [24]. SK values should ideally be zero at these frequencies where Gaussian noise exists and an extremely positive value at frequencies where transitory signals appear. Therefore, SK can be utilized to detect signal frequency boundaries and thus address issues of EWT.

In this paper, an optimized noise reduction method of PD fluorescence fiber sensors is proposed to overcome the spectrum segmentation drawbacks of conventional EWT. Firstly, the optimized EWT introduces SK to determine compact supports of the Fourier spectrum of PD fluorescence signal, which can significantly reduce redundant mode components division. Subsequently, adaptive wavelet threshold denoising is used to eliminate residual noise in the reconstructed signal, so as to obtain a denoised PD fluorescence signal. The proposed method is validated through numerically simulated and experimentally obtained PD fluorescence signal, and it is further analyzed in comparison with the novel adaptive ensemble EMD (NAEEMD) method, EWT method, EWT joint with kurtogram (KEWT) method, and correlation spectral negentropy (CSNE)-based method, which demonstrates its denoising effectiveness in fluorescence fiber sensors.

## II. PRINCIPLE OF THE PROPOSED METHOD

### A. Spectral Kurtosis (SK)

Based on the Wold-Cramér decomposition theory, SK can be determined by energy-normalized fourth-order spectral cumulant [23]

$$K_x(f) = \frac{\langle |H(k, f)|^4 \rangle}{\langle |H(k, f)|^2 \rangle^2} - 2, f \neq 0, \quad (1)$$

where  $H(k, f)$  is complex envelope of non-stationary process  $x(k)$  at frequency  $f$ ,  $\langle \cdot \rangle$  denotes the temporal average operator.

Short-time Fourier transform (STFT) is commonly used to estimate SK values. However, the window length  $N_w$  utilized in STFT has a significant impact on this STFT-based SK estimation approach [23]. As a result, selecting the appropriate window length  $N_w$  to maximize SK values is critical. To obtain the optimal window length  $N_w^*$ , SK calculation for all potential window lengths needs to be performed, which is computationally expensive. Fortunately, a fast kurtogram (FK) can quickly determine the kurtosis of each frequency sub-band. The principle of FK is based on a 1/3-binary tree of filter bank structure. A detailed process is available in [25]. The maximum kurtosis value in the kurtogram can be used to find the optimal window length  $N_w^*$ .

Since the optimal window length  $N_w^*$  has been identified, SK values of noisy PD fluorescence signal are estimated using the STFT-based approach. To further clarify frequency regions

where the PD fluorescence signal is located, it is essential to compare SK values with a statistic threshold  $s_\alpha$ , which is defined as [26]

$$s_\alpha = \Phi^{-1}(\alpha) \frac{2}{\sqrt{M}}, \quad (2)$$

where  $\Phi^{-1}(\alpha)$  is the quantile function of standard normal distribution,  $\alpha$  is the confidence level used to evaluate whether the signal is non-stationary or stationary, and  $M$  is the number of elements along the time axis in  $H(k, f)$ . Frequency components with SK values greater than threshold  $s_\alpha$  are referred to as the PD fluorescence signal, while those with SK values less than threshold  $s_\alpha$  belong to Gaussian noise. Consequently, SK is capable of being used to identify the frequency band where the PD fluorescence signal is located.

### B. Empirical Wavelet Transform (EWT)

The principle of EWT is to construct  $N$  filter banks (one lowpass and  $N-1$  bandpass filters) to extract intrinsic mode components with compact support from the Fourier spectrum of the signal [19]. As a result, the EWT procedure contains two critical steps: segmenting the signal Fourier spectrum and constructing matching wavelet filters to process the signal.

Assuming that the Fourier spectrum  $[0, \pi]$  is continuously split into  $N$  segments, the boundary limits of each segment are denoted as  $\omega_n$  (where  $\omega_0 = 0$ , and  $\omega_N = \pi$ ). Each segment is represented as  $\Lambda_n = [\omega_{n-1}, \omega_n]$ , viz.  $\cup_{n=1}^N \Lambda_n = [0, \pi]$ . Subsequently, filter banks are defined on each  $\Lambda_n$  utilizing the idea of Littlewood-Paley and Meyer's wavelets. The empirical scaling function  $\hat{\phi}_1(\omega)$  and empirical wavelet function  $\hat{\psi}_n(\omega)$  are expressed as follows, respectively [19]:

$$\hat{\phi}_1(\omega) = \begin{cases} 1 & \text{if } |\omega| \leq (1 - \gamma) \omega_1 \\ \cos \left[ \frac{\pi}{2} \beta \left( \frac{1}{2\gamma\omega_1} (|\omega| - (1 - \gamma) \omega_1) \right) \right] & \text{if } (1 - \gamma) \omega_1 \leq |\omega| \leq (1 + \gamma) \omega_1 \\ 0 & \text{otherwise,} \end{cases} \quad (3)$$

$$\hat{\psi}_n(\omega) = \begin{cases} 1 & \text{if } (1 + \gamma) \omega_n \leq |\omega| \leq (1 - \gamma) \omega_{n+1} \\ \cos \left[ \frac{\pi}{2} \beta \left( \frac{1}{2\gamma\omega_{n+1}} (|\omega| - (1 - \gamma) \omega_{n+1}) \right) \right] & \text{if } (1 - \gamma) \omega_{n+1} \leq |\omega| \leq (1 + \gamma) \omega_{n+1} \\ \sin \left[ \frac{\pi}{2} \beta \left( \frac{1}{2\gamma\omega_n} (|\omega| - (1 - \gamma) \omega_n) \right) \right] & \text{if } (1 - \gamma) \omega_n \leq |\omega| \leq (1 + \gamma) \omega_n \\ 0 & \text{otherwise,} \end{cases} \quad (4)$$

where  $\gamma < \min_n \left( \frac{\omega_{n+1} - \omega_n}{\omega_{n+1} + \omega_n} \right)$  and auxiliary function  $\beta(x)$  is defined as

$$\beta(m) = \begin{cases} 0 & \text{if } m \leq 0 \\ m^4 (35 - 84m + 70m^2 - 20m^3) & \text{if } 0 \leq m \leq 1 \\ 1 & \text{if } m \geq 1. \end{cases} \quad (5)$$

Therefore, the original signal  $x(t)$  is reconstructed as

$$x(t) = F^{-1} \left[ \hat{W}_f^\varepsilon(0, \omega) \cdot \hat{\phi}_1(\omega) + \sum_{n=1}^{N-1} \hat{W}_f^\varepsilon(n, \omega) \cdot \hat{\psi}_n(\omega) \right], \quad (6)$$

where  $\hat{W}_f^\varepsilon(0, \omega)$  and  $\hat{W}_f^\varepsilon(n, \omega)$  are the Fourier transform of approximation coefficients and detail coefficients, respectively, and  $F^{-1}[\cdot]$  represents the inverse Fourier transform operator.

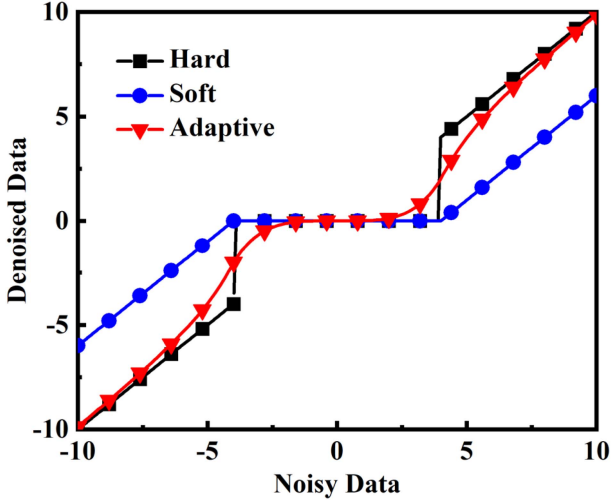


Fig. 1. Comparison of the adaptive wavelet threshold function with the hard and soft threshold functions.

### C. Adaptive Wavelet Threshold Denoising

Noise information in the noisy fluorescence signal cannot be completely eliminated after EWT decomposition and reconstruction. Given the subsequent necessity to calculate the PD quantity using the waveform integration approach, residual noise can impair the accuracy of the calculation [6], [27]. Thus, an appropriate wavelet threshold function is essential in the noise reduction process. Hard and soft threshold functions are the ones that are most frequently employed [28]. However, the hard threshold function is discontinuous, resulting in a certain fluctuation of the denoised signal. While the soft threshold function is continuous in contrast to the hard threshold function, it introduces deviations in signal reconstruction. To address the current shortcomings, a novel wavelet threshold function is introduced in this paper, which is based on the hard and soft threshold functions. This threshold function is shown as follows:

$$w'(k) = \begin{cases} w(k) - \frac{\lambda^4}{2 \cdot (w(k))^3}, & |w(k)| > \lambda \\ \frac{\text{sgn}(w(k)) \cdot (w(k))^4}{2 \cdot \lambda^3}, & |w(k)| \leq \lambda, \end{cases} \quad (7)$$

where  $\text{sgn}(\cdot)$  represents the sign function operator, and  $\lambda$  is the wavelet threshold. The adaptive threshold function is contrasted with the hard and soft threshold functions, as depicted in Fig. 1. It is obvious that the adaptive wavelet threshold function is continuous, thus avoiding signal fluctuations. Meanwhile, when  $|w(k)|$  is greater than  $\lambda$ , the deviation between  $w'(k)$  and  $w(k)$  diminishes as  $w(k)$  increases, which enhances the accuracy of signal reconstruction.

In addition, the selection of wavelet threshold  $\lambda$  is also quite crucial. Borrowed from the idea of median absolute deviation in outlier detection [29], the vast majority of time domain points in the noisy PD fluorescence signal can be deemed as noise, whereas a small percentage of points are the PD fluorescence signal, i.e., outliers. Hence, wavelet threshold  $\lambda$  is defined as follows [30]:

$$\lambda = 2.5 \cdot MAD + \text{med}(X), \quad (8)$$

$$MAD = 1.4826 \cdot \text{med}(|X - \text{med}(X)|), \quad (9)$$

where  $X$  represents the original observation, and  $\text{med}(\cdot)$  denotes the median operator.

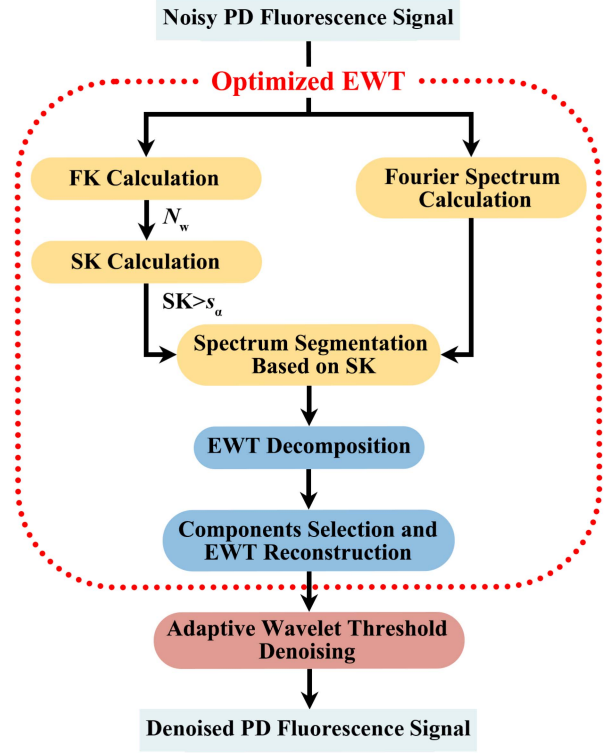


Fig. 2. Flowchart of the proposed method.

### D. The Proposed Method

To obviate inappropriate segmentation in conventional EWT, the optimized EWT based on SK segmentation is proposed. The main procedures of the proposed denoising method are depicted in Fig. 2.

- 1) Determine the optimal window length  $N_w^*$  by calculating the FK of the noisy PD fluorescence signal  $x(n)$ . Subsequently, calculate the SK of the noisy PD fluorescence signal at  $N_w^*$ .
- 2) Find frequency components with SK values greater than threshold  $s_\alpha$ , which are considered as the PD fluorescence signal. Especially, employ the endpoints of these frequency components as boundaries. Split the Fourier spectrum using boundaries based on SK values.
- 3) Decompose the noisy PD fluorescence signal utilizing filter banks based on the empirical scale function and empirical wavelet function. Select frequency components with SK values over the statistic threshold  $s_\alpha$  for EWT reconstruction.
- 4) Calculate wavelet threshold  $\lambda$  and subsequently further denoise the reconstructed signal by applying the adaptive wavelet threshold denoising to obtain the denoised PD fluorescence signal.

## III. SIMULATION ANALYSIS

### A. Simulated PD Fluorescence Signal

The PD detection method utilizing fluorescence fiber sensors is based on the fluorescence intensity of PMT output. The excitation of PD light enables many particles to initially be excited, which causes fluorescence to be intense at first [31]. Following that, fluorescence steadily diminishes, exhibiting a

TABLE I  
SIMULATED PD FLUORESCENCE PULSE PARAMETERS

Pulse	P1	P2	P3	P4	Units
$A$	0.8	1.3	2	0.8	mV
$\tau_1$	3	3	0.8	1.5	$\mu\text{s}$
$\tau_2$	0.5	0.5	0.1	0.3	$\mu\text{s}$

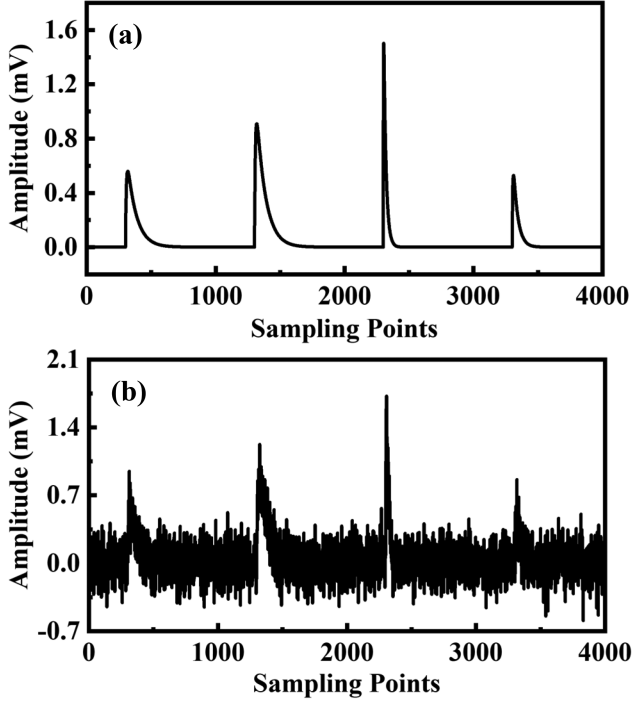


Fig. 3. Simulated PD fluorescence signal: (a) Noise-free PD signal and (b) noisy PD signal.

double-exponential decline trend. Therefore, the PD fluorescence signal can be evaluated by a double exponential decay pulse, which is denoted as follows [32]:

$$s(t) = A \cdot \left( e^{-\frac{1.3t}{\tau_1}} - e^{-\frac{2.2t}{\tau_2}} \right), \quad (10)$$

where  $A$  is the pulse amplitude,  $\tau_1$  and  $\tau_2$  are the attenuation coefficients. In this paper, four PD pulses are simulated with various parameter combinations. The specific parameters are listed in Table I. Furthermore, the sampling frequency  $f_s$  is 30 MHz. Gaussian white noise is added to the noise-free PD fluorescence signal to achieve a signal-to-noise ratio (SNR) of 0 dB. The noise-free and noisy PD fluorescence signals are depicted in Fig. 3.

### B. Analysis of Simulation Result

Firstly, the FK of the noisy PD fluorescence signal is determined, as illustrated in Fig. 4(a). Since the kurtosis achieves its maximum at level 4.6, the optimal window length  $N_w^*$  is 48. Subsequently, the SK of the noisy PD fluorescence signal is calculated at the optimal window length  $N_w^*$ , and the results are presented in Fig. 4(b). The calculated threshold  $s_\alpha$  is 0.3128. Endpoints of frequency components with SK values higher than

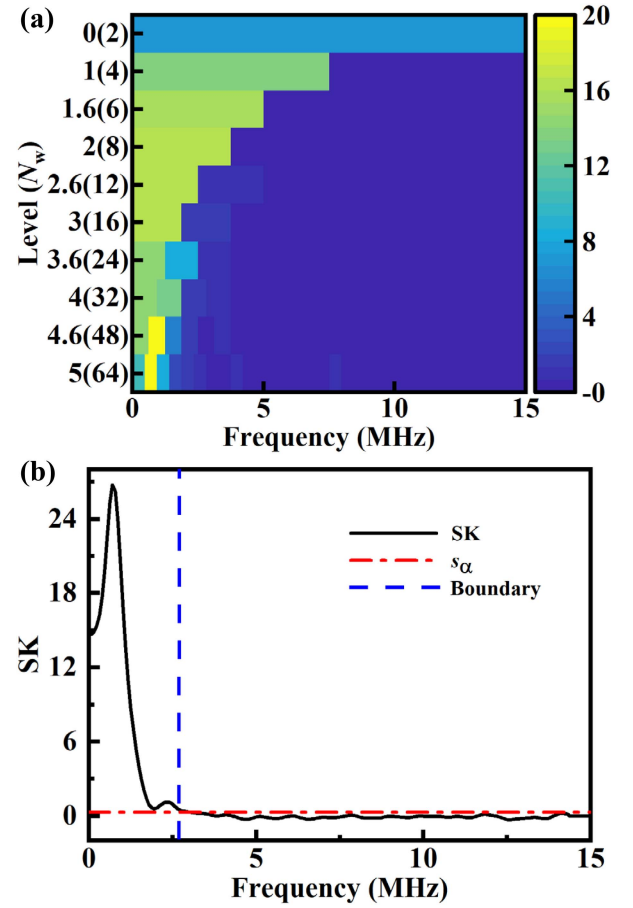


Fig. 4. (a) FK of the noisy PD fluorescence signal. (b) Spectrum segmentation based on SK at the optimal window length  $N_w^*$ .

threshold  $s_\alpha$  serve as the boundaries. Consequently, the acquired boundaries allow the Fourier spectrum to be automatically separated into two components, one of which with SK values greater than threshold  $s_\alpha$  represents the PD fluorescence signal and the other the noise.

The noisy PD fluorescence signal is decomposed using filter banks constructed with acquired boundaries and the EWT decomposition results are depicted in Fig. 5. It is evident that the PD fluorescence signal fundamentally exists in component  $C_1$ , while the noise is predominantly concentrated in component  $C_2$ . Since the SK values of component  $C_1$  are greater than threshold  $s_\alpha$ , component  $C_1$  is selected for EWT reconstruction. Subsequently, the reconstructed signal is further processed by the adaptive wavelet threshold denoising described in Section II. And the estimated wavelet threshold  $\lambda$  is 0.2081. The final denoised PD fluorescence signal can be obtained after the adaptive wavelet threshold denoising.

The denoising results of the proposed method are compared to those of the NAEEMD method [17], EWT method [20], [21], KEWT method [33], and CSNE-based method [34], [35], in order to validate its performance. The corresponding denoising results are displayed in Fig. 6. Despite addressing the modal mixing issue, the NAEEMD method and EWT method still retain a significant amount of noise and can only hazily identify the PD signal, which are depicted in Fig. 6(a) and (b), therefore,

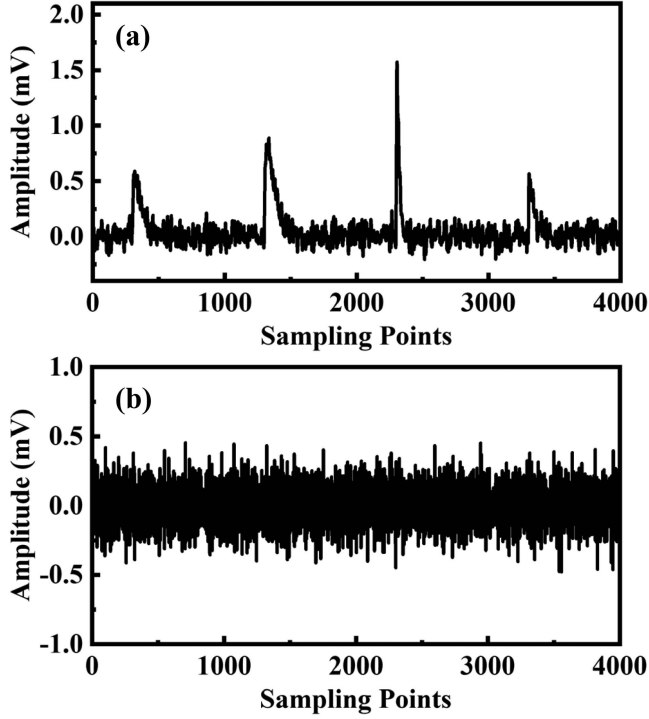


Fig. 5. EWT decomposition results with the proposed method: (a) component  $C_1$  and (b) component  $C_2$ .

their noise suppression performance is not satisfactory. The KEWT method and CSNE-based method can effectively reduce white noise, with the KEWT method demonstrating superior denoising performance compared to the CSNE-based method, as shown in Fig. 6(c) and (d), but the pulse waveform in Fig. 6(c) exhibits a severe truncation phenomenon, which is attributed to the determination of the starting and ending positions of PD pulses, as well as the discontinuity of the hard threshold function. In contrast to the previous four methods, it is shown that the proposed method successfully suppresses noise while preserving signal detail. Meanwhile, there is less distortion in the waveform of the denoised PD fluorescence signal in Fig. 6(d).

To quantify the noise reduction performance of the proposed method, several evaluation metrics are introduced, including root-mean-square error (RMSE), normalized correlation coefficient (NCC), and SNR [20]:

$$RMSE = \sqrt{\frac{1}{N_{\text{len}}} \sum_{k=1}^{N_{\text{len}}} [y(k) - s(k)]^2}, \quad (11)$$

$$NCC = \frac{\sum_{k=1}^{N_{\text{len}}} s(k) \cdot y(k)}{\sqrt{\left[ \sum_{k=1}^{N_{\text{len}}} s(k)^2 \right] \cdot \left[ \sum_{k=1}^{N_{\text{len}}} y(k)^2 \right]}}, \quad (12)$$

$$SNR = 10 \log_{10} \left( \frac{\sum_{k=1}^{N_{\text{len}}} s(k)^2}{\sum_{k=1}^{N_{\text{len}}} [y(k) - s(k)]^2} \right), \quad (13)$$

where  $s$  and  $y$  are the noise-free and denoised PD fluorescence signals, respectively, and  $N_{\text{len}}$  is the length of these signals. In general, superior noise reduction performance is indicated by higher NCC and SNR values, as well as lower RMSE values.

The evaluation metrics of various denoising methods with different  $SNR_0$  are listed in Table II. All the computation involved in this paper is executed on an Intel Core processor (i7-8700 @ 3.2 GHz) employing Matlab R2022b. The NAEEMD method performs better at high  $SNR_0$ , but not as well as the other methods at low  $SNR_0$ . The denoising performance of the KEWT method outperforms the EWT method, especially in low  $SNR_0$  scenarios. The CSNE-based method exhibits prominent denoising effectiveness at high  $SNR_0$ , but its performance deteriorates compared to KEWT at low  $SNR_0$ . Given the lower RMSE, higher NCC, and higher SNR values of the proposed method, it is obvious that this proposed method has less waveform distortion and surpasses the competition in terms of denoising capability. Meanwhile, the denoising results of the proposed method are still significant even with a low  $SNR_0$  ( $SNR_0 = -5$  dB), proving its adaptability to harsher environments. Furthermore, the NAEEMD method requires a considerable amount of computational time, since it decomposes the signals by superimposing multiple times auxiliary white noise, which is not conducive to the real-time processing of fluorescence signals. Due to the fine segmentation being performed, the EWT method is still time-consuming, but the processing time is less than that of the NAEEMD method. The calculation time of the proposed method is comparable to that of the KEWT method and relatively short. Hence, this proposed method has the virtue of providing a superior denoising effect while still being computationally efficient.

## IV. EXPERIMENTAL RESULTS AND DISCUSSION

### A. Experimental Setup

To verify the noise reduction effect of the proposed method, an actual PD fluorescence signal with noise is acquired in the laboratory. In our previous work [6], the PD experimental measurement platform has been constructed, as illustrated in Fig. 7. A power-frequency transformer with a maximum voltage of 50 kV serves as the high-voltage source. The protective resistance has a resistive value of 5 k $\Omega$  and the voltage divider has a voltage ratio of 1000:1. Corona discharge is produced utilizing a needle-plate model, which is placed in an opaque black plexiglass tank. The homemade cerium and terbium co-doped silica fiber (CTDSF) [6], [36] sensor is placed in the tank and connected to PMT (H10722-210, Hamamatsu Photonics, Japan) via silica transmission fiber. The CTDSF sensor absorbs the PD light (mainly between 210 and 400 nm) and converts it to visible light, which is transmitted via transmission fiber to the PMT for detection. Subsequently, the high-speed digital oscilloscope (MSO8204, Rigol, China) with a sampling rate of 50 MSa/s is utilized to acquire the PMT output signals.

### B. Results and Discussion

The measured noisy PD fluorescence signal acquired by the CTDSF sensor is shown in Fig. 8. It is obvious that the PD fluorescence signal is severely hampered by the intense background noise present in the environment. The FK and SK of the measured noisy PD fluorescence signal are depicted in Fig. 9. The optimal window length  $N_w^*$  and statistic threshold  $s_\alpha$  are 96 and 0.2793, respectively. Therefore, two compact supports of the

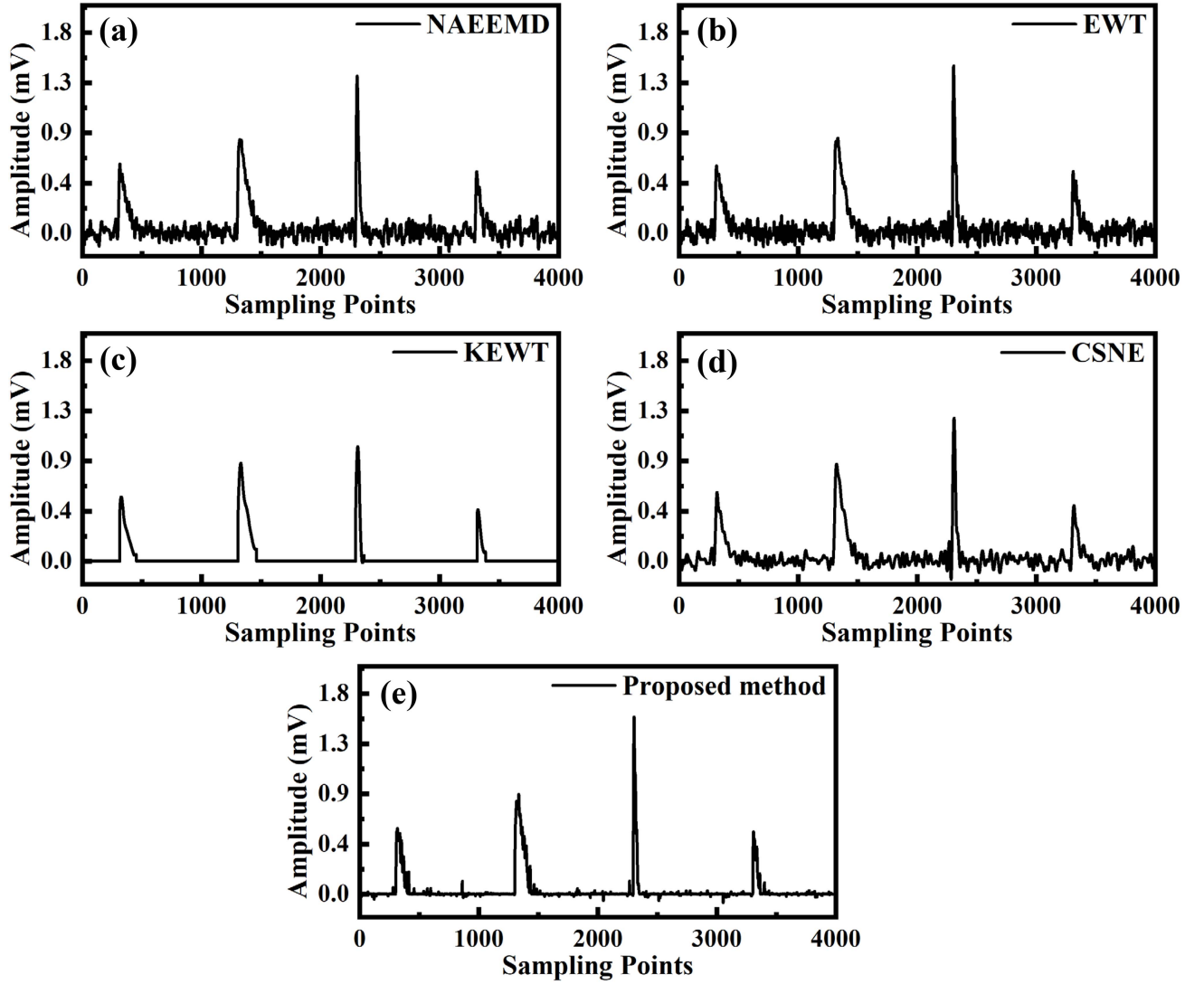


Fig. 6. Denoising results of the simulated signal with different methods with  $\text{SNR}_0 = 0$  dB (a) NAEEMD, (b) EWT, (c) KEWT, (d) CSNE, and (e) proposed method.

TABLE II  
EVALUATION METRICS COMPARISON OF VARIOUS DENOISING METHODS WITH DIFFERENT  $\text{SNR}_0$

$\text{SNR}_0/\text{dB}^a$	Methods	RMSE	NCC	$\text{SNR}_d/\text{dB}^b$	Time/s
0	NAEEMD	0.0560	0.9388	8.8699	5.5204
	EWT	0.0586	0.9350	8.4813	1.6478
	KEWT	0.0585	0.9269	8.4957	0.3111
	CSNE	0.0487	0.9516	10.0893	0.5375
	Proposed method	0.0352	0.9742	12.9217	0.3517
-3	NAEEMD	0.0795	0.8918	5.8353	5.3390
	EWT	0.0843	0.8789	5.3201	1.6784
	KEWT	0.0593	0.9247	8.3857	0.3137
	CSNE	0.0653	0.9165	7.5428	0.5943
	Proposed method	0.0414	0.9641	11.5081	0.3591
-5	NAEEMD	0.0754	0.8964	6.2883	5.2634
	EWT	0.0890	0.8688	4.8488	1.6853
	KEWT	0.0650	0.9088	7.5855	0.3147
	CSNE	0.0690	0.9069	7.0586	0.6441
	Proposed method	0.0469	0.9536	10.4207	0.3625

<sup>a</sup> $\text{SNR}_0$  is the signal-to-noise ratio of the noisy signal. <sup>b</sup> $\text{SNR}_d$  is the signal-to-noise ratio of the denoised signal.

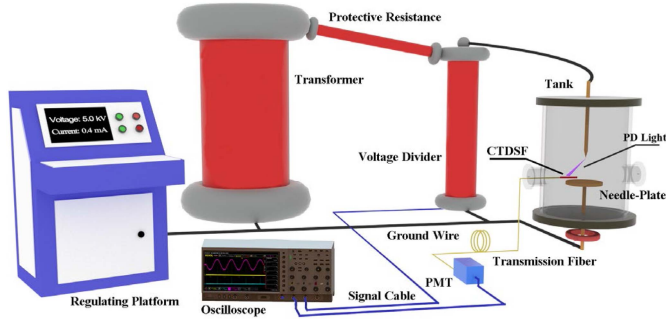


Fig. 7. Experimental setup utilizing the CTDSF sensor for PD fluorescence detection.

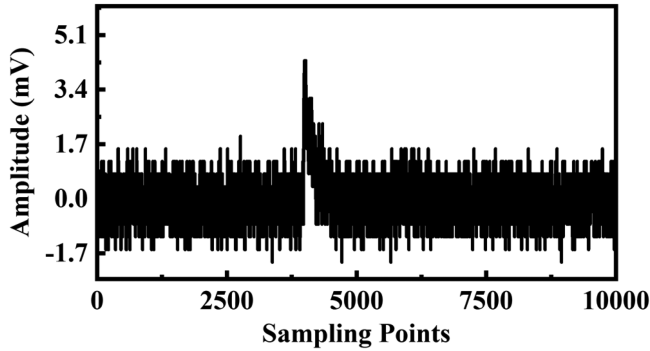


Fig. 8. The measured noisy PD fluorescence signal.

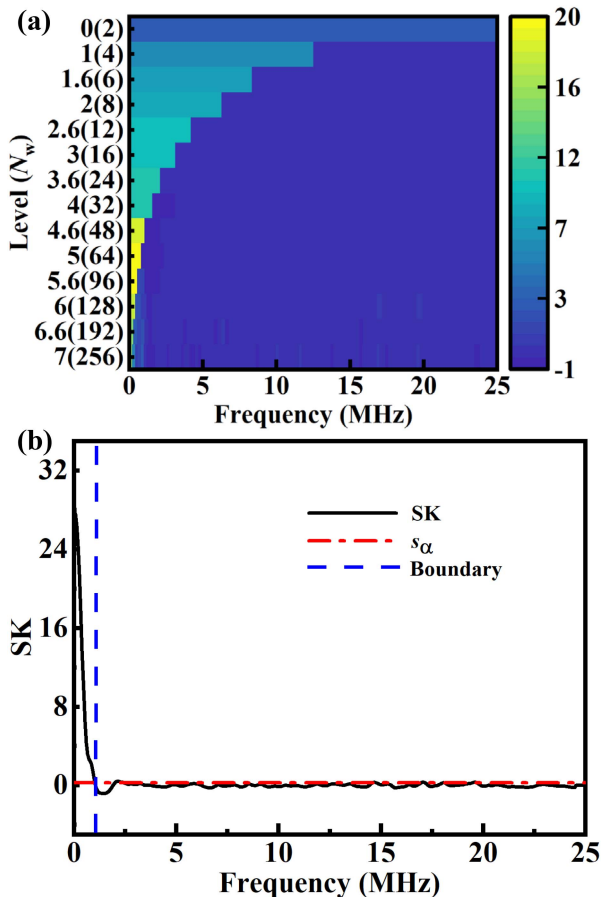


Fig. 9. (a) FK of the measured noisy PD fluorescence signal. (b) SK of the measured noisy PD fluorescence signal at  $N_w = 96$ .

TABLE III  
EVALUATION METRICS COMPARISON OF THE MEASURED NOISY PD FLUORESCENCE SIGNAL

	NAEEMD	EWT	KEWT	CSNE	Proposed method
NRR	1.9292	4.5462	8.4441	4.0426	6.0829
SCL	0.4077	0.1739	0.2218	0.2564	0.6497
Time/s	15.9277	19.9681	0.3719	1.9109	0.4329

signal spectrum can be obtained after spectrum segmentation based on SK. The denoised PD fluorescence signal is then acquired via the optimized EWT and adaptive wavelet threshold denoising.

The above denoising methods are still employed to process the measured noisy PD fluorescence signal in order to compare the denoising performance, and the denoising results are depicted in Fig. 10. All these denoising methods can identify the PD fluorescence signal. The NAEEMD, EWT, and CSNE-based method can all extract fluorescence signals, with the EWT and CSNE-based method demonstrating better performance, however, all these three methods still retain significant amounts of noise, thus making them unsuitable for handling weak PD signals. Meanwhile, the denoised PD signal processed by the KEWT method suffers from severe waveform distortion because the noise interferes with the judgment of the end position of the PD pulse. Notably, the proposed method recovers the PD fluorescence signal somewhat better than the other four methods, which helps with further PD localization or pattern identification.

Since the noise-free PD fluorescence signal cannot be obtained in the practical detection, the evaluation metrics described above are not applicable to the measured noisy PD fluorescence signal. Consequently, the noise reduction ratio (NRR) is introduced to evaluate the denoising performance of the measured PD fluorescence signal, which is defined as [37]

$$NRR = 10 \cdot (\lg \sigma_1^2 - \lg \sigma_2^2), \quad (14)$$

where  $\sigma_1^2$  and  $\sigma_2^2$  are the variance of the noisy signal and denoised signal, respectively. A higher NRR value is typically associated with better denoising performance. However, when  $\sigma_2^2$  is close to 0, it will incorrectly indicate the denoising result. Therefore, in order to characterize the denoising effect of the measured signal, the statistical consistency level (SCL) and NRR are coupled in this paper, which is defined as [38]

$$SCL = kstest2[\text{Re}(F(x-y)), \text{Im}(F(x-y))], \quad (15)$$

where  $x$  and  $y$  are the noisy signal and denoised signal, respectively,  $F(\cdot)$  denotes the fast Fourier transform operator,  $\text{Re}(\cdot)$  and  $\text{Im}(\cdot)$  represent the real part and imaginary part of complex numbers, and  $kstest2(\cdot)$  is the Kolmogorov Smirnov test operator. It can be seen that the denoising result improves with increasing SCL.

The NRR and SCL metrics and execution time comparison of the measured noisy PD fluorescence signal are listed in Table III. Despite having the highest NRR, the denoising effect of the KEWT method is not satisfactory. Therefore, focusing solely on the NRR metric is insufficient for the measured PD fluorescence signal. By comparing the NRR and SCL metrics, the proposed method achieves a maximum SCL of 0.6497 while maintaining a significant NRR of 6.0829, which indicates its better noise suppression effect. In addition, the KEWT and proposed method

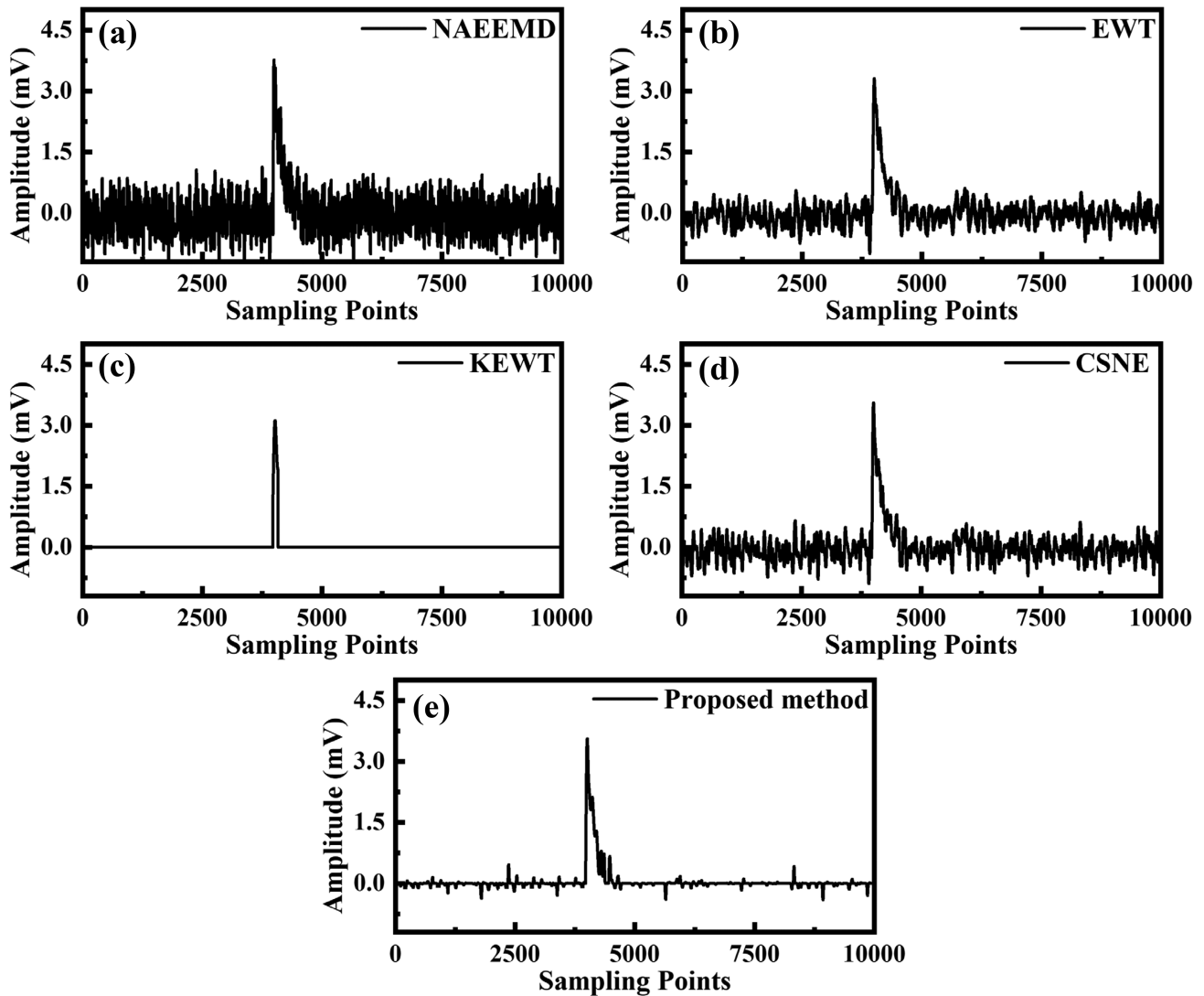


Fig. 10. Denoising results of the measured noisy PD fluorescence signal with different methods. (a) NAEEMD, (b) EWT, (c) KEWT, (d) CSNE, and (e) proposed method.

have relatively low execution time when compared to the other three methods. It can be observed that the proposed method can work well on the measured PD fluorescence signal with CTDSF sensors.

## V. CONCLUSION

The present research proposes a self-adaptive noise reduction method for PD fluorescence fiber sensors based on optimized EWT and adaptive wavelet threshold denoising. Firstly, the optimized EWT improves the Fourier spectrum division efficiency of conventional EWT by utilizing the SK at the optimal window length, which significantly reduces the computational cost of the algorithm. The reconstructed signal is obtained using compact supports with SK values greater than the statistic threshold, thus removing the majority of the noise. Secondly, the adaptive wavelet threshold denoising is exploited to suppress the remaining noise in the reconstructed signal. The denoising results of the proposed method are analyzed for numerically simulated and experimentally obtained PD fluorescence signals,

which demonstrates that the proposed method is capable of accurately extracting PD fluorescence signals and suppressing noise. Furthermore, the proposed method's denoising results are compared qualitatively and quantitatively to those of the other four denoising methods (NAEEMD, EWT, KEWT, and CSNE-based method), revealing that the proposed method has a low computational cost and outperforms the other four methods in terms of noise suppression and signal detail maintenance. The usage of the proposed method is promising for broadening applications of fluorescence fiber sensors in the PD detection field.

## REFERENCES

- [1] W. Zhang, P. Lu, W. Ni, W. Z. Xiong, D. Liu, and J. S. Zhang, "Gold-diaphragm based Fabry-Perot ultrasonic sensor for partial discharge detection and localization," *IEEE Photon. J.*, vol. 12, no. 3, Jun. 2020, Art. no. 6801612, doi: [10.1109/JPHOT.2020.2982460](https://doi.org/10.1109/JPHOT.2020.2982460).
- [2] P. Zhu, H. Q. Wen, Q. Che, and X. Y. Li, "Disturbed partial discharge detection system based on an improved  $\Phi$ -OTDR assisted by a wFBG array," *Appl. Opt.*, vol. 59, no. 14, pp. 4367–4370, May 2020, doi: [10.1364/AO.380554](https://doi.org/10.1364/AO.380554).



- [3] X. Hu, W. H. Siew, M. D. Judd, A. J. Reid, and B. Sheng, "Modeling of high-frequency current transformer based partial discharge detection in high-voltage cables," *IEEE Trans. Power Del.*, vol. 34, no. 4, pp. 1549–1556, Aug. 2019, doi: [10.1109/TPWRD.2019.2910076](https://doi.org/10.1109/TPWRD.2019.2910076).
- [4] H. Li, J. Lv, D. Li, C. Xiong, Y. Zhang, and Y. Yu, "MEMS-on-fiber ultrasonic sensor with two resonant frequencies for partial discharges detection," *Opt. Exp.*, vol. 28, no. 12, pp. 18431–18439, Jun. 2020, doi: [10.1364/OE.391242](https://doi.org/10.1364/OE.391242).
- [5] R. V. de Andrade Lira et al., "Elliptical UHF sensor for partial discharge detection," *Sensors Actuators A: Phys.*, vol. 348, Dec. 2022, Art. no. 113981, doi: [10.1016/j.sna.2022.113981](https://doi.org/10.1016/j.sna.2022.113981).
- [6] C. Hu et al., "An innovative fluorescent fiber sensor based on Ce/Tb codoped silica fiber for partial discharge detection," *IEEE Sensors J.*, vol. 23, no. 7, pp. 6939–6947, Apr. 2023, doi: [10.1109/JSEN.2023.3248236](https://doi.org/10.1109/JSEN.2023.3248236).
- [7] S. J. S. Tsai, "Power transformer partial discharge (PD) acoustic signal detection using fiber sensors and wavelet analysis, modeling, and simulation," M.S. thesis, Dept. Elect. Comput. Eng., Virginia Tech, Blacksburg, VA, USA, 2002. [Online]. Available: <http://hdl.handle.net/10919/35983>
- [8] X. Han et al., "Partial discharge detection in gas-insulated switchgears using sensors integrated with UHF and optical sensing methods," *IEEE Trans. Dielectrics Elect. Insul.*, vol. 29, no. 5, pp. 2026–2033, Oct. 2022, doi: [10.1109/TDEI.2022.3198715](https://doi.org/10.1109/TDEI.2022.3198715).
- [9] W. Zhang et al., "An optical fiber Fabry-Perot interferometric sensor based on functionalized diaphragm for ultrasound detection and imaging," *IEEE Photon. J.*, vol. 9, no. 3, Jun. 2017, Art. no. 7103208, doi: [10.1109/JPHOT.2017.2694480](https://doi.org/10.1109/JPHOT.2017.2694480).
- [10] Q. Zhang et al., "High-sensitivity EFPI-based acoustic sensor using in-fiber collimator and adjustable 45° mirror," *IEEE Photon. J.*, vol. 16, no. 2, Apr. 2024, Art. no. 6800507, doi: [10.1109/JPHOT.2024.3363020](https://doi.org/10.1109/JPHOT.2024.3363020).
- [11] A. A. Soltani and S. M. Shahrtash, "Decision tree-based method for optimum decomposition level determination in wavelet transform for noise reduction of partial discharge signals," *Int. Eng. Technol. Sci. Meas. Technol.*, vol. 14, no. 1, pp. 9–16, Jan. 2020, doi: [10.1049/iet-smt.2019.0081](https://doi.org/10.1049/iet-smt.2019.0081).
- [12] Q. Lin, F. Lyu, S. Yu, H. Xiao, and X. Li, "Optimized denoising method for weak acoustic emission signal in partial discharge detection," *IEEE Trans. Dielectrics Elect. Insul.*, vol. 29, no. 4, pp. 1409–1416, Aug. 2022, doi: [10.1109/TDEI.2022.3183662](https://doi.org/10.1109/TDEI.2022.3183662).
- [13] W. Sun, S. Zhu, W. Li, W. Chen, and N. Zhu, "Noise suppression of distributed acoustic sensing based on f-x deconvolution and wavelet transform," *IEEE Photon. J.*, vol. 12, no. 1, Feb. 2020, Art. no. 7800208, doi: [10.1109/JPHOT.2020.2972645](https://doi.org/10.1109/JPHOT.2020.2972645).
- [14] Y. W. Tang, C. C. Tai, C. C. Su, C. Y. Chen, and J. F. Chen, "A correlated empirical mode decomposition method for partial discharge signal denoising," *Meas. Sci. Technol.*, vol. 21, no. 8, Jun. 2010, Art. no. 085106, doi: [10.1088/0957-0233/21/8/085106](https://doi.org/10.1088/0957-0233/21/8/085106).
- [15] X. J. Chen and Y. M. Yang, "Analysis of the partial discharge of ultrasonic signals in large motor based on Hilbert-Huang transform," *Appl. Acoust.*, vol. 131, pp. 165–173, Feb. 2018, doi: [10.1016/j.apacoust.2017.10.028](https://doi.org/10.1016/j.apacoust.2017.10.028).
- [16] J. C. Chan, H. Ma, T. K. Saha, and C. Ekanayake, "Self-adaptive partial discharge signal de-noising based on ensemble empirical mode decomposition and automatic morphological thresholding," *IEEE Trans. Dielectrics Elect. Insul.*, vol. 21, no. 1, pp. 294–303, Feb. 2014, doi: [10.1109/TDEI.2013.003839](https://doi.org/10.1109/TDEI.2013.003839).
- [17] T. Jin, Q. Li, and M. A. Mohamed, "A novel adaptive EEMD method for switchgear partial discharge signal denoising," *IEEE Access*, vol. 7, pp. 58139–58147, 2019, doi: [10.1109/ACCESS.2019.2914064](https://doi.org/10.1109/ACCESS.2019.2914064).
- [18] S. Zhang et al., "An adaptive CEEMDAN thresholding denoising method optimized by nonlocal means algorithm," *IEEE Trans. Instrum. Meas.*, vol. 69, no. 9, pp. 6891–6903, Sep. 2020, doi: [10.1109/TIM.2020.2978570](https://doi.org/10.1109/TIM.2020.2978570).
- [19] J. Gilles, "Empirical wavelet transform," *IEEE Trans. Signal Proces.*, vol. 61, no. 16, pp. 3999–4010, Aug. 2013, doi: [10.1109/TSP.2013.2265222](https://doi.org/10.1109/TSP.2013.2265222).
- [20] J. Zhong, X. Bi, Q. Shu, M. Chen, D. Zhou, and D. K. Zhang, "Partial discharge signal denoising based on singular value decomposition and empirical wavelet transform," *IEEE Trans. Instrum. Meas.*, vol. 69, no. 11, pp. 8866–8873, Nov. 2020, doi: [10.1109/TIM.2020.2996717](https://doi.org/10.1109/TIM.2020.2996717).
- [21] R. Liang, Z. Zhang, H. L. Li, P. Chi, G. X. Li, and Y. C. Tao, "Partial discharge location of power cables based on an improved single-terminal method," *Electric Power Syst. Res.*, vol. 193, Apr. 2021, Art. no. 107013, doi: [10.1016/j.epsr.2020.107013](https://doi.org/10.1016/j.epsr.2020.107013).
- [22] Y. Hu, F. C. Li, H. G. Li, and C. L. Liu, "An enhanced empirical wavelet transform for noisy and non-stationary signal processing," *Digit. Signal Process.*, vol. 60, pp. 220–229, Jan. 2017, doi: [10.1016/j.dsp.2016.09.012](https://doi.org/10.1016/j.dsp.2016.09.012).
- [23] J. Antoni, "The spectral kurtosis: A useful tool for characterising non-stationary signals," *Mech. Syst. Signal Process.*, vol. 20, no. 2, pp. 282–307, Feb. 2006, doi: [10.1016/j.ymsp.2004.09.001](https://doi.org/10.1016/j.ymsp.2004.09.001).
- [24] K. Yu, T. R. Lin, J. W. Tan, and H. Ma, "An adaptive sensitive frequency band selection method for empirical wavelet transform and its application in bearing fault diagnosis," *Measurement*, vol. 134, pp. 375–384, Feb. 2019, doi: [10.1016/j.measurement.2018.10.086](https://doi.org/10.1016/j.measurement.2018.10.086).
- [25] J. Antoni, "Fast computation of the kurtogram for the detection of transient faults," *Mech. Syst. Signal Process.*, vol. 21, no. 1, pp. 108–124, Jan. 2007, doi: [10.1016/j.ymsp.2005.12.002](https://doi.org/10.1016/j.ymsp.2005.12.002).
- [26] J. Antoni and R. B. Randall, "The spectral kurtosis: Application to the vibratory surveillance and diagnostics of rotating machines," *Mech. Syst. Signal Process.*, vol. 20, no. 2, pp. 308–331, Feb. 2006, doi: [10.1016/j.ymsp.2004.09.002](https://doi.org/10.1016/j.ymsp.2004.09.002).
- [27] A. Rodrigo, P. Llovera, V. Fuster, and A. Quijano, "Study of partial discharge charge evaluation and the associated uncertainty by means of high frequency current transformers," *IEEE Trans. Dielectrics Elect. Insul.*, vol. 19, no. 2, pp. 434–442, Apr. 2012, doi: [10.1109/TDEI.2012.6180236](https://doi.org/10.1109/TDEI.2012.6180236).
- [28] H. Liu, W. D. Wang, C. L. Xiang, L. J. Han, and H. Z. Nie, "A de-noising method using the improved wavelet threshold function based on noise variance estimation," *Mech. Syst. Signal Process.*, vol. 99, pp. 30–46, Jan. 2018, doi: [10.1016/j.ymsp.2017.05.034](https://doi.org/10.1016/j.ymsp.2017.05.034).
- [29] C. Leys, C. Ley, O. Klein, P. Bernard, and L. Licata, "Detecting outliers: Do not use standard deviation around the mean, use absolute deviation around the median," *J. Exp. Social Psychol.*, vol. 49, no. 4, pp. 764–766, Jul. 2013, doi: [10.1016/j.jesp.2013.03.013](https://doi.org/10.1016/j.jesp.2013.03.013).
- [30] H. Fitriyah and A. S. Budi, "Outlier detection in object counting based on hue and distance transform using median absolute deviation (MAD)," in *Proc. Int. Conf. Sustain. Inf. Eng. Technol.*, 2019, pp. 217–222, doi: [10.1109/SIET48054.2019.8985993](https://doi.org/10.1109/SIET48054.2019.8985993).
- [31] J. L. Zheng, X. L. Wu, Q. Ren, Y. H. Ren, and O. Hai, "Luminescence properties, energy transfer and thermal stability of blue-green color tunable Sr<sub>3</sub>Y(BO<sub>3</sub>)<sub>3</sub>:Ce<sup>3+</sup>, Tb<sup>3+</sup> phosphors," *Opt. Laser Technol.*, vol. 123, Mar. 2020, Art. no. 105900, doi: [10.1016/j.optlastec.2019.105900](https://doi.org/10.1016/j.optlastec.2019.105900).
- [32] Y. N. Li and Z. H. Li, "Application of a novel wavelet shrinkage scheme to partial discharge signal denoising of large generators," *Appl. Sci.*, vol. 10, no. 6, Mar. 2020, Art. no. 2162, doi: [10.3390/app10062162](https://doi.org/10.3390/app10062162).
- [33] J. Zhong, X. Bi, Q. Shu, D. Zhang, and X. Li, "An improved wavelet spectrum segmentation algorithm based on spectral kurtogram for denoising partial discharge signals," *IEEE Trans. Instrum. Meas.*, vol. 70, 2021, Art. no. 3514408, doi: [10.1109/TIM.2021.3071224](https://doi.org/10.1109/TIM.2021.3071224).
- [34] K. Zhang, Y. G. Xu, Z. Q. Liao, L. Y. Song, and P. Chen, "A novel fast entropygram and its applications in rolling bearing fault diagnosis," *Mech. Syst. Signal Process.*, vol. 154, Jun. 2021, Art. no. 107582, doi: [10.1016/j.ymsp.2020.107582](https://doi.org/10.1016/j.ymsp.2020.107582).
- [35] K. Zhang, P. Chen, M. R. Yang, L. Y. Song, and Y. G. Xu, "The Harmonogram: A periodic impulses detection method and its application in bearing fault diagnosis," *Mech. Syst. Signal Process.*, vol. 165, Feb. 2022, Art. no. 108374, doi: [10.1016/j.ymsp.2021.108374](https://doi.org/10.1016/j.ymsp.2021.108374).
- [36] M. Jia et al., "Tapered fiber radiation sensor based on Ce/Tb:YAG crystals for remote gamma-ray dosimetry," *Opt. Exp.*, vol. 29, no. 2, pp. 1210–1220, Jan. 2021, doi: [10.1364/OE.413822](https://doi.org/10.1364/OE.413822).
- [37] C. Z. Fang, Y. S. Chen, X. L. Deng, X. L. Lin, Y. Han, and J. J. Zheng, "Denoising method of machine tool vibration signal based on variational mode decomposition and Whale-Tabu optimization algorithm," *Sci. Rep.*, vol. 13, no. 1, Jan. 2023, Art. no. 1505, doi: [10.1038/s41598-023-28404-7](https://doi.org/10.1038/s41598-023-28404-7).
- [38] C. Wang, C. X. Yu, Q. Shu, D. K. Zhang, and Y. H. He, "Noise suppression in PD signal based on Prony time series energy spectrum," *Int. Eng. Technol. Sci. Meas. Technol.*, vol. 16, no. 1, pp. 1–14, Sep. 2022, doi: [10.1049/smt2.12076](https://doi.org/10.1049/smt2.12076).